

# $\mathcal{PT}$ restoration via increased loss-gain in $\mathcal{PT}$ -symmetric Aubry-Andre model

Charles Liang, Derek D. Scott, and Yogesh N. Joglekar

Department of Physics, Indiana University Purdue University Indianapolis (IUPUI), Indianapolis, Indiana 46202, USA

(Dated: February 12, 2014)

In systems with “balanced loss and gain”, the  $\mathcal{PT}$ -symmetry is broken by increasing the non-hermiticity or the loss-gain strength. We show that finite lattices with oscillatory,  $\mathcal{PT}$ -symmetric potentials exhibit a new class of  $\mathcal{PT}$ -symmetry breaking and restoration. We obtain the  $\mathcal{PT}$  phase diagram as a function of potential periodicity, which also controls the location complex eigenvalues in the lattice spectrum. We show that the sum of  $\mathcal{PT}$ -potentials with nearby periodicities leads to  $\mathcal{PT}$ -symmetry restoration, where the system goes from a  $\mathcal{PT}$ -broken state to a  $\mathcal{PT}$ -symmetric state as the average loss-gain strength is increased. We discuss the implications of this novel transition for the propagation of a light in an array of coupled waveguides.

*Introduction.* Open systems with balanced loss and gain have gained tremendous interest in the past three years since their experimental realizations in optical [1–4], electrical [5], and mechanical [6] systems. Such systems are described by non-hermitian Hamiltonians that are invariant under combined parity and time-reversal ( $\mathcal{PT}$ ) operations [7]. Apart from their mathematical appeal, such non-hermitian Hamiltonians show non-intuitive properties such as unidirectional invisibility [4, 8, 9] and are thus of potential technological importance.

Historically,  $\mathcal{PT}$  Hamiltonians on an infinite line were the first to be investigated [10, 11]. The range of parameters where the spectrum of the Hamiltonian is purely real,  $\epsilon_\lambda = \epsilon_\lambda^*$ , and the eigenfunctions are simultaneous eigenfunctions of the  $\mathcal{PT}$  operator,  $\psi_\lambda(x) = \psi_\lambda^*(-x)$ , is called the  $\mathcal{PT}$ -symmetric phase. The emergence of complex conjugate eigenvalues when the parameters are not in this region is called  $\mathcal{PT}$ -symmetry breaking. A positive threshold for  $\mathcal{PT}$ -symmetry breaking implies that the system transitions [2–6] from a quasi-equilibrium state at a small but nonzero non-hermiticity, to loss of reciprocity as the strength of the balanced loss-gain term crosses the threshold. Although  $\mathcal{PT}$ -symmetric Hamiltonian studies started with continuum Hamiltonians, all of their realizations are in finite lattices where the continuum, effective-mass approximation may not apply. This observation has led to tremendous interest in  $\mathcal{PT}$ -symmetric lattice models [12–18] that can be realized in coupled waveguide arrays [19, 20].

A universal feature of all such systems is that  $\mathcal{PT}$ -symmetry is broken by increasing the balanced loss-gain strength and restored by reducing it. Here, we present a tight-binding model that can exhibit exactly opposite behavior, via a family of  $\mathcal{PT}$ -symmetric, periodic potentials.

A remarkable property of lattice models, absent in the continuum limit, is the effects of a periodic potential. The spectrum of a charged particle in constant magnetic field in two dimensions consists of Landau levels [21–23]; a similar particle on a two-dimensional lattice displays a fractal, Hofstadter butterfly spectrum [24–27]. In one dimensional lattices, a fractal spectrum

emerges in the presence of a hermitian, periodic potential, and this model, known as the Aubry-Andre model [28], shows localization transition in a clean system when the strength of the incommensurate potential exceeds the nearest-neighbor hopping [29]. Here, we consider a  $\mathcal{PT}$ -symmetric Aubry-Andre model on an  $N$ -site lattice with hopping  $J$  and complex potential  $V_\beta(n) = V_0 \cos[2\pi\beta(n - n_c)] + i\gamma \sin[2\pi\beta(n - n_c)]$  where  $n_c = (N + 1)/2$  is the lattice center and  $\gamma > 0$ . Since  $V_\beta = (-1)^{2n_c} V_{1-\beta}^* = (-1)^{2n_c} V_{1+\beta}$ , it is sufficient to consider the family of potentials with  $0 < \beta < 1$  (when  $\beta = 0$  the problem reduces to the Aubrey-Andre model [24, 28]). We then consider the effect of two such potentials  $V_{\beta_1} + V_{\beta_2}$  with  $|\beta_1 - \beta_2| \sim 1/N \ll 1$ .

Our salient results are follows: i) For a single potential  $V_\beta$ , the threshold loss-gain strength  $\gamma_{PT}(N, V_0, \beta)$  shows  $N$  local maxima along the  $\beta$  axis; it is suppressed by a nonzero real modulation  $V_0$ . ii) The discrete index of pair of eigenvalues that become complex can be tuned stepwise by varying  $0 < \beta < 1/2$ . iii) For  $V = V_{\beta_1} + V_{\beta_2}$ , generically, the phase diagram in the  $(\gamma_1, \gamma_2)$  plane shows a re-entrant  $\mathcal{PT}$ -symmetric phase: a broken  $\mathcal{PT}$ -symmetry is restored by increasing the non-hermiticity and broken again when  $\gamma_i$  become sufficiently large. This behavior is absent in the extensively studied continuum Hamiltonians with complex potentials [30–32], and is a result of competition between the two lattice potentials  $V_{\beta_1}$  and  $V_{\beta_2}$ .

We emphasize that  $\gamma_i > 0$  means the gain-regions of the two potentials mostly align as do their respective loss-regions. Thus, the competition between  $V_{\beta_1}$  and  $V_{\beta_2 \approx \beta_1}$  is not in their loss-gain profiles, but, as we will show below, due to the relative locations of  $\mathcal{PT}$ -symmetry breaking energy-levels in the spectrum.

*$\mathcal{PT}$  phase diagram for a single potential.* The tight-binding hopping Hamiltonian for an  $N$ -site lattice with open boundary conditions is  $H_0 = -J \sum_{n=1}^{N-1} (|n\rangle\langle n+1| + |n+1\rangle\langle n|)$ . Its particle-hole symmetric energy spectrum is given by  $\epsilon_{0,p} = -2J \cos(k_p) = -\epsilon_{0,\bar{p}}$  and the corresponding normalized eigenfunctions are  $\psi_p(j) = \sin(k_p j) = (-1)^j \sin(k_{\bar{p}} j)$  where  $0 < k_p = p\pi/(N+1) < \pi$  and  $\bar{p} = N + 1 - p$ . The properties that relate eigenval-

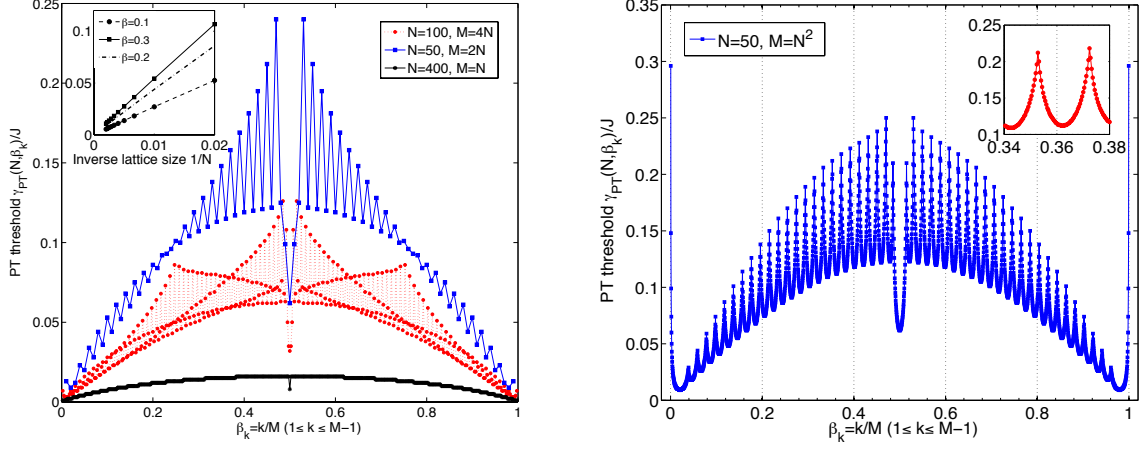


FIG. 1. (color online) Left-hand panel:  $\mathcal{PT}$ -symmetric threshold  $\gamma_{PT}(N, \beta)$  for  $N = 50$  lattice with discretization  $\beta_k = k\delta\beta = k/2N$  (blue squares),  $N = 100$  lattice with  $\delta\beta = 1/4N$  (red markers), and  $N = 400$  lattice with  $\delta\beta = 1/N$  (black stars) shows that the phase-diagram depends sensitively on  $\delta\beta \sim O(1/N)$ . The inset shows that for a fixed  $\beta$ , the threshold is linearly suppressed,  $\gamma_{PT}(N, \beta) = C_\beta/N$ . Right-hand panel: Results are independent of the discretization when  $\delta\beta \sim 1/N^2 \ll 1/N$  and the  $N = 50$  phase-diagram shows  $N$  local maxima and smooth oscillations with period  $\Delta\beta = 1/N$  (inset).

ues and eigenfunctions at indices  $p, \bar{p}$  remain valid in the presence of pure loss-gain potential  $V_\beta = -V_\beta^*$  [33]. The eigenvalue equation for an eigenfunction  $f(n)$  of the non-Hermitian,  $\mathcal{PT}$ -symmetric Hamiltonian  $H_\beta = H_0 + V_\beta$  is given by ( $1 \leq n \leq N$ )

$$-J[f(n+1) + f(n-1)] + V_\beta(n)f(n) = Ef(n), \quad (1)$$

with  $f(0) = 0 = f(N+1)$ . Since this difference equation is not analytically soluble for an arbitrary  $\beta$ , we numerically obtain the spectrum  $E(\gamma)$  and the  $\mathcal{PT}$ -symmetry breaking threshold  $\gamma_{PT}(N, V_0, \beta)$  using different discretizations  $\beta_k = k\delta\beta$  along the  $\beta$ -axis. Due to the  $\beta \leftrightarrow 1 - \beta$  symmetry of the potential, it follows that the exact threshold loss-gain strength satisfies  $\gamma_{PT}(N, V_0, \beta) = \gamma_{PT}(N, V_0, 1 - \beta) = \gamma_{PT}(N, -V_0, \beta)$ .

We consider a purely loss-gain potential, present results for an even lattice, and point out the salient differences that arise when lattice size  $N$  is odd or when  $V_0 \neq 0$ . The left-hand panel in Fig. 1 shows the  $\mathcal{PT}$ -symmetric threshold  $\gamma_{PT}(N, \beta)/J$  for an  $N = 50$  lattice obtained by using discretization  $\delta\beta = 1/2N$  (blue squares), an  $N = 100$  lattice with  $\delta\beta = 1/4N$  (red markers), and an  $N = 400$  lattice with  $\delta\beta = 1/N$  (black stars). There is a monotonic suppression of the threshold strength with increasing  $N$ , and, crucially, the general shape of the phase diagram depends upon the size of  $\delta\beta$  relative to  $1/N$ . A scaling of this threshold suppression for lattice sizes  $N = 50 - 500$ , shown in the inset, implies that  $\gamma_{PT}(N, \beta) = C_\beta/N$  where  $C_\beta$  is a constant. Thus, the threshold strength is suppressed linearly and vanishes in the thermodynamic limit [34, 35]. However, this algebraically fragile nature of the  $\mathcal{PT}$ -phase is not an impediment since  $\mathcal{PT}$ -systems to-date are only realized

in small lattices with  $N \ll 100$ . The right-hand panel in Fig. 1 shows the phase diagram for  $N = 50$  case with discretization  $\delta\beta = 1/N^2$ . The results for irrational values of  $\beta$  and other discretizations lie on the same curve. The  $\mathcal{PT}$  phase diagram shows  $(N - 2)$  local maxima located at  $\beta_k = (2k + 1)/2N$  and the two maxima at the end points, is symmetric about the center and has a local minimum in the threshold at  $\beta = 1/2$ . In addition, the function  $\gamma_{PT}(N, \beta)$  has  $(N - 1)$  minima at  $\beta_k = k/N$  and smoothly oscillates over a period  $\sim 1/N = 0.02$  as shown in the inset (solid red circles). These results are generic for any lattice size  $N$  with discretization  $\delta\beta \sim 1/N^2$ .

When  $N$  is odd, the non-Hermitian potential vanishes at  $\beta = 1/2$  and the spectrum of the Hamiltonian  $H_\beta$  is purely real. For an odd lattice, a similarly obtained phase diagram shows  $(N - 1)$  local maxima that are distributed equally on the two sides of  $\beta = 1/2$ , along with a substantial enhancement in the threshold strength as  $\beta \rightarrow 1/2^\pm$ . Adding a real potential modulation  $V_0 \neq 0$ , to the loss-gain potential, in general, suppresses the threshold strength.

The phase diagram can be understood as follows: for a small  $\beta \sim 1/N^2 \ll 1/N$ ,  $V_\beta(n) = i\gamma(2\pi\beta)(n - n_c)$  and the enhanced  $\mathcal{PT}$ -breaking threshold,  $\gamma_{PT}/J \sim 0.3$ , is consistent with a linear-potential threshold [36]. For an even lattice, the average of the gain-potential is given by  $A_E(\beta) = \sum_{n>n_c}^N V_\beta(n)/i\gamma = \sin^2(N\pi\beta/2)/\sin(\pi\beta) \geq 0$ . The  $\mathcal{PT}$  threshold is greatest when the *change in the average strength is maximum* as  $\beta$  is varied,  $\partial_\beta^2 A_E(\beta) = 0$ . In the limit  $N \gg 1$  and  $\beta \gg 1/N^2$ , it implies that the  $N$  maxima of  $\gamma_{PT}(N, \beta)$  occur at  $\beta_{k,\max} = (2k+1)/2N$ . On the other hand,  $\gamma_{PT}(N, \beta)$  is smallest when the *change in the average strength is minimum*,  $\partial_\beta A_E(\beta) = 0$ , and gives

the locations of  $(N-1)$  minima as  $\beta_{k,\min} = k/N$ . A similar analysis applies to odd lattices, where the average potential is given by  $A_O(\beta) = \sin[\pi\beta(N-1)/2] \sin[\pi\beta(N+1)/2] / \sin(\pi\beta)$ .

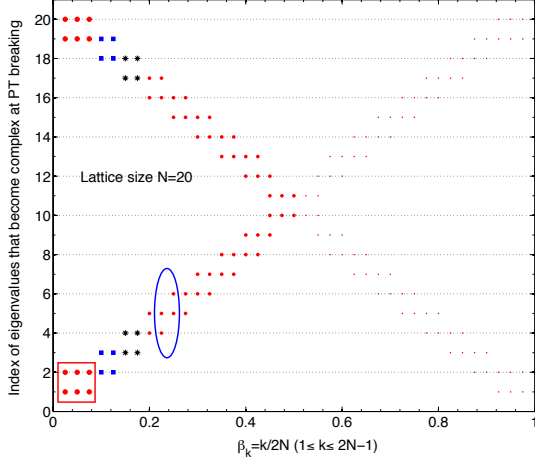


FIG. 2. (color online) Index of eigenvalues that become complex as a function of  $\beta$  for an  $N = 20$  lattice with discretization  $\delta\beta = 1/2N = 0.025$  shows a  $\beta \leftrightarrow 1 - \beta$  symmetry, denoted by heavy and light red markers. When  $\beta \leq 0.08$ , levels  $(E_1, E_2)$  become degenerate and complex, and so do their particle-hole counterparts,  $(E_{19}, E_{20})$  (red circles); in general, we can tune the location of  $\mathcal{PT}$ -breaking (blue squares, black stars, red markers) by appropriately choosing  $\beta$ .

Next, we focus on the *location* of the  $\mathcal{PT}$  symmetry breaking. Due to the particle-hole symmetric spectrum of  $H_\beta$ , two pairs of levels  $(E_n, E_{n+1})$  and  $(-E_n, -E_{n+1})$  become complex simultaneously. Figure 2 plots the indices of eigenvalues that become complex as a function of  $\beta$  for an  $N = 20$  lattice with discretization  $\delta\beta = 1/2N$ . It shows that at small  $\beta$ , the eigenvalues at the band edges become complex, whereas, as  $\beta \rightarrow 1/2$ , the pairs of eigenvalues that become complex move to the center of the band. Thus the average range of  $\beta$ s with the same location for  $\mathcal{PT}$ -symmetry breaking is  $\sim 1/N$ . It follows that by choosing an appropriate  $\beta$ , one is able to control the location of  $\mathcal{PT}$ -symmetry breaking in the energy spectrum. As we will see next, this control allows us to introduce competition between potentials  $V_\beta$  with two different, but close, values of  $\beta$ .

**$\mathcal{PT}$  phase diagram with two potentials.** We now consider the  $\mathcal{PT}$ -symmetric phase of the Hamiltonian with two potentials,  $H = H_0 + V_{\beta_1} + V_{\beta_2}$ , in the  $(\gamma_1, \gamma_2)$  plane, where both axes are scaled by their respective threshold values  $\gamma_{jPT} = \gamma_{PT}(\beta_j)$ . Panel (a) in Fig. 3 shows the numerically obtained phase diagram for an  $N = 20$  lattice with  $(\beta_1, \beta_2) = (0.20, 0.25)$  (blue stars and squares). It shows that, from a  $\mathcal{PT}$ -broken phase (point 1), it is possible to enter the  $\mathcal{PT}$ -symmetric phase by increasing the non-hermiticity  $\gamma_1$  (point 2). We emphasize that increas-

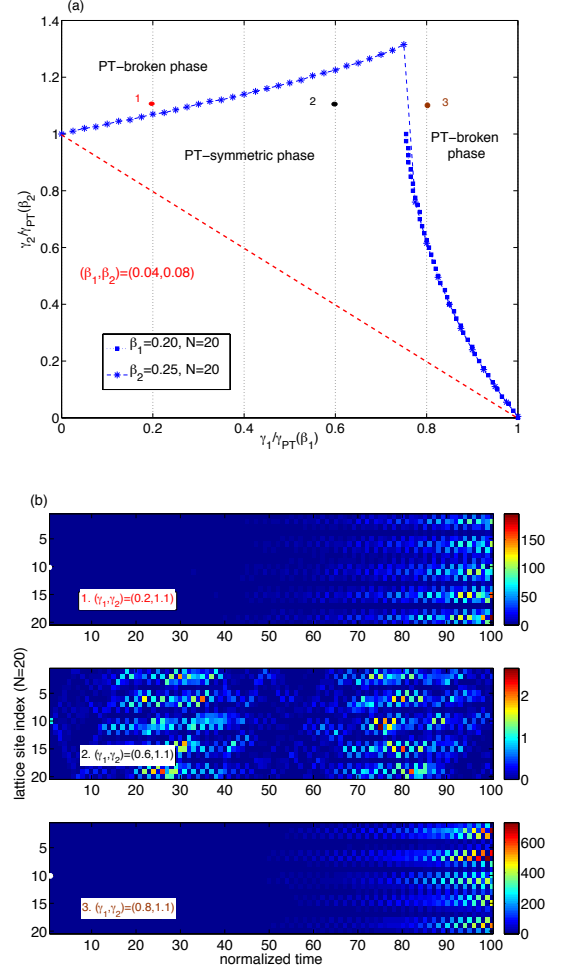


FIG. 3. (color online) Panel (a):  $\mathcal{PT}$ -phase diagram for potential  $V_{\beta_1} + V_{\beta_2}$ . When  $(\beta_1, \beta_2) = (0.20, 0.24)$  (blue stars and squares), a  $\mathcal{PT}$ -broken phase (point 1) is restored by increasing  $\gamma_1$  (point 2) and subsequently broken again (point 3). This re-entrant phase is due to competition between  $V_{\beta_1}$  and  $V_{\beta_2}$ . For  $(\beta_1, \beta_2) = (0.04, 0.08)$ , the two co-operate and the phase boundary is an expected straight line. Panel (b): intensity  $I(k, t)$  of an initially normalized state shows that, starting from a  $\mathcal{PT}$ -broken phase (top panel), increasing  $\gamma_1$  initially restores bounded oscillations (center panel), followed by  $\mathcal{PT}$  breaking and amplification (bottom panel). Note the two-orders-of-magnitude difference in the total intensity.

ing  $\gamma_1$  increases the average gain- (and loss-) strength  $\gamma_1 A_E(\beta_1) + \gamma_2 A_E(\beta_2)$ , and yet drives the system into a  $\mathcal{PT}$ -symmetric phase from a  $\mathcal{PT}$ -broken phase. Increasing  $\gamma_1$  further, eventually, drives the system into a  $\mathcal{PT}$  broken phase again (point 3).

While a  $\mathcal{PT}$ -broken phase implies an exponential time-dependence of the net intensity or the norm of a state, in the  $\mathcal{PT}$ -symmetric phase the net intensity oscillates within a bound that is determined by the proximity of the Hamiltonian to the  $\mathcal{PT}$  phase boundary [20]. Panel (b) in Fig. 3 shows the dramatic consequences of  $\mathcal{PT}$

restoration on the site- and time-dependent intensity  $I(k, t) = |\langle k | \exp(-iHt/\hbar) | \psi_0 \rangle|^2$  of a state  $|\psi_0\rangle$  that is initially localized on site  $N/2 = 10$ ; the time is measured in units of  $\hbar/J$ . The top-subpanel shows that intensity has a monotonic amplification in regions with gain sites, leading to a striated pattern (point 1). Center subpanel shows that by increasing  $\gamma_1$ , oscillatory behavior in the intensity is restored (point 2). Bottom subpanel shows that increasing  $\gamma_1$  further breaks the  $\mathcal{PT}$  symmetry again (point 3). Thus, we are able to *restore  $\mathcal{PT}$ -symmetry by increasing the non-hermiticity*, and achieve amplification by both reducing or increasing the average gain-strength. This novel behavior is absent in all lattice models with a single  $\mathcal{PT}$  potential.

Since each potential  $V_{\beta_j}$  breaks the  $\mathcal{PT}$  symmetry for  $\gamma_j/\gamma_{jPT} > 1$ , naively, one may expect that the  $\mathcal{PT}$  phase boundary for  $V_{\beta_1} + V_{\beta_2}$  is given by  $\gamma_1/\gamma_{1PT} + \gamma_2/\gamma_{2PT} = 1$ . This is indeed the case for  $(\beta_1, \beta_2) = (0.04, 0.08)$ , shown by red dashed line in panel (a), even though the potential periodicities differ by a factor of two.

What is the key difference between the two sets of parameters, one of which shows a re-entrant  $\mathcal{PT}$ -symmetric phase? It is the indices of eigenvalues that become complex due to  $V_{\beta_1}$  and  $V_{\beta_2}$ . The red rectangle in Fig. 2 shows that for  $\beta \leq 0.8$ , eigenvalues ( $E_1, E_2$ ) become complex. In such a case, the two potentials  $V_{\beta_1}$  and  $V_{\beta_2}$  act in a cooperative manner effectively adding their strengths. Therefore, the  $\mathcal{PT}$ -phase boundary is a straight line. In contrast, the blue oval in Fig. 2 shows that for  $\beta_1 = 0.20$ , energy levels  $E_4, E_5$  approach each other, become degenerate, and then complex as  $\gamma \rightarrow \gamma_{1PT}$ ; for  $\beta_2 = 0.25$ , the energy levels that become complex as  $\gamma \rightarrow \gamma_{2PT}$  are  $E_5, E_6$ . Thus, the level  $E_5$  is *lowered by potential  $V_{\beta_1}$  and raised by the potential  $V_{\beta_2}$*  from its hermitian-limit value. This introduces competition between the two potentials  $V_{\beta_1}$  and  $V_{\beta_2}$  even though their gain-regions largely overlap and so do their respective loss regions.

This correspondence between competing potentials and  $\mathcal{PT}$ -restoration is further elucidated in Fig. 4. In conjunction with Fig. 2, it shows that re-entrant  $\mathcal{PT}$ -symmetric phase occurs when the two potentials compete (panels b-e, g, h). This restoration of  $\mathcal{PT}$ -symmetry can be due to increased loss-gain strength in  $\gamma_1$  (panels d, e),  $\gamma_2$  (panels b, c, g), or both (panel h). On the other hand, when the two potentials break the same set of eigenvalues, the  $\mathcal{PT}$  phase boundary is a line (panels a, f, k).

*Discussion.* Competing potentials, a common theme in physics, often stabilize phases that would be unstable in the presence of only one of them [37]. A trivial definition of competing  $\mathcal{PT}$ -potentials is that the gain-region of one strongly overlaps with the loss-region of another, thus reducing the average gain (and loss) strength.

Here, we have unmasked the subtle competition between  $\mathcal{PT}$  potentials whose gain regions largely overlap, based on the location of  $\mathcal{PT}$ -symmetry breaking induced by each. This competition results in  $\mathcal{PT}$ -restoration and

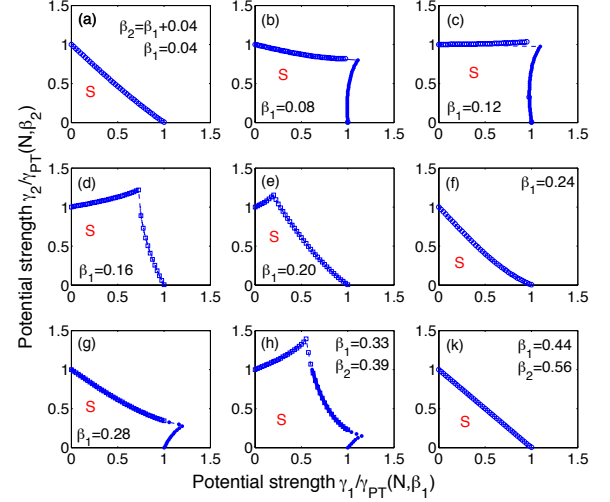


FIG. 4. (color online)  $\mathcal{PT}$ -phase boundary for an  $N = 20$  lattice with potentials  $V_{\beta_1} + V_{\beta_2}$  shows that  $\mathcal{PT}$ -symmetry restoration can occur by increasing non-hermiticity  $\gamma_1$  (panels b, c, g),  $\gamma_2$  (panels d, e), or both (panel h) when the two potentials compete. When they make complex the same set of eigenvalues, the phase boundary is a line (panels a, f, k). The label “S” denotes the  $\mathcal{PT}$ -symmetric phase.

subsequent  $\mathcal{PT}$ -breaking, leading to selective intensity suppression and oscillations at large loss-gain strength. Its hints were seen in a continuum model with complex  $\delta$ -function and constant potentials, but that continuum model is neither easily experimentally realizable nor can it tune between cooperative and competitive behavior [39]. The  $\mathcal{PT}$ -symmetric Aubry-Andre model provides a family of potentials with tunable competition or cooperation among them, and is thus ideal for investigating the consequences of such competition; even lattices as small as  $N = 10$  that can be realized via coupled optical waveguides [19, 20] or cold atoms [38] may provide a comprehensive understanding of interplay between loss-gain strengths and  $\mathcal{PT}$ -symmetry breaking.

This work was supported by NSF Grant No. DMR-1054020.

- 
- [1] A. Guo, G.J. Salamo, D. Duchesne, R. Morandotti, M. Volatier-Ravat, V. Aimez, G.A. Siviloglou, and D.N. Christodoulides, Phys. Rev. Lett. **103**, 093902 (2009).
  - [2] C.E. Rüter, K.G. Makris, R. El-Ganainy, D.N. Christodoulides, M. Segev, and D. Kip, Nat. Phys. **6**, 192 (2010).
  - [3] L. Feng, M. Ayache, J. Huang, Y.-L. Xu, M.-H. Lu, Y.-F. Chen, Y. Fainman, and A. Scherer, Science **333**, 729 (2011).
  - [4] A. Regensburger, C. Bersch, M.-A. Miri, G. Onishchukov, D.N. Christodoulides, and U. Peschel, Nature **488**, 167 (2012).

- [5] J. Schindler, A. Li, M.C. Zheng, F.M. Ellis, and T. Kottos, Phys. Rev. A **84**, 040101(R) (2011).
- [6] C.M. Bender, B.K. Berntson, D. Parker, and E. Samuel, Am. J. Phys. **81**, 173 (2013).
- [7] For a review, see C.M. Bender, Rep. Prog. Phys. **70**, 947 (2007) and references therein.
- [8] Z. Lin, H. Ramezani, T. Eichelkraut, T. Kottos, H. Cao, and D.N. Christodoulides, Phys. Rev. Lett. **106**, 213901 (2011).
- [9] L. Feng, Y.-L. Xu, W.S. Fegadolli, M.-H. Lu, J.E.B. Oliveira, V.R. Almeida, Y.-F. Chen, and A. Scherer, Nat. Mater. **12**, 108 (2013).
- [10] C.M. Bender and S. Boettcher, Phys. Rev. Lett. **80**, 5243 (1998).
- [11] C.M. Bender, D.C. Brody, and H.F. Jones, Phys. Rev. Lett. **89**, 270401 (2002).
- [12] M. Znojil, Phys. Rev. A **82**, 052113 (2010).
- [13] M. Znojil, Phys. Lett. A **375**, 3435 (2011).
- [14] O. Bendix, R. Fleischmann, T. Kottos, and B. Shapiro, Phys. Rev. Lett. **103**, 030402 (2009).
- [15] L. Jin and Z. Song, Phys. Rev. A **80**, 052107 (2009).
- [16] Y.N. Joglekar and A. Saxena, Phys. Rev. A **83**, 050101(R) (2011).
- [17] G. Della Valle and S. Loghi, Phys. Rev. A **87**, 022119 (2013).
- [18] S. Longhi, G. Della Valle, Ann. Phys. **334**, 35 (2013).
- [19] D.N. Christodoulides, F. Lederer, and Y. Silberberg, Nature (London) **424**, 817 (2003).
- [20] Y.N. Joglekar, C. Thompson, D.D. Scott, and G. Vemuri, Eur. Phys. J. Appl. Phys. **63**, 30001 (2013).
- [21] See chapter XV, L.D. Landau and E.M. Lifshitz, *Quantum Mechanics (Non-relativistic Theory)* (Butterworth-Heinemann, Burlington, MA, 2005).
- [22] F.D.M. Haldane, Phys. Rev. Lett. **61**, 2015 (1988).
- [23] Y. Zheng and T. Ando, Phys. Rev. B **65**, 245420 (2002).
- [24] P. Harper, Proc. Phys. Soc. London Sec. A **68**, 874 (1955).
- [25] D. Hofstadter, Phys. Rev. B **14**, 2239 (1976).
- [26] M. Aidelsburger, M. Atala, M. Lohse, J. T. Barreiro, P. Paredes, and I. Bloch, Phys. Rev. Lett. **111**, 185301 (2013); H. Miyake, G.A. Siviloglou, C.J. Kennedy, W.C. Burton, and W. Ketterle, *ibid* 185302 (2013).
- [27] L.A. Ponomarenko *et al.*, Nature (London) **497**, 594 (2013); C.R. Dean *et al.*, *ibid* 598 (2013).
- [28] S. Aubry and G. Andre, Ann. Isr. Phys. Soc. **3**, 133 (1980).
- [29] Y. Lahini, R. Pugatch, F. Pozzi, M. Sorel, R. Morandotti, N. Davidson, and Y. Silberberg, Phys. Rev. Lett. **103**, 013901 (2009).
- [30] K.G. Makris, R. El-Ganainy, D.N. Christodoulides, Z.H. Musslimani, Phys. Rev. Lett. **100**, 103904 (2008).
- [31] S. Longhi, Phys. Rev. A **81**, 022102 (2010).
- [32] E.-M. Graefe and H.F. Jones, Phys. Rev. A **84**, 013818 (2011).
- [33] Y.N. Joglekar, Phys. Rev. A **82**, 044101 (2010).
- [34] Y.N. Joglekar, D. Scott, M. Babbey, and A. Saxena, Phys. Rev. A **82**, 030103(R) (2010).
- [35] D.E. Pelinovsky, P.G. Kevrekidis, and D.J. Frantzeskakis, EPL **101**, 11002 (2013).
- [36] M. Serbyn, M.A. Skvortsov, Phys. Rev. B **87**, 020501 (2013).
- [37] See, for example, E. Fradkin, *Field Theories of Condensed Matter Systems* (Addison Wesley, Reading, MA, 1991).
- [38] H. Li, J. Dou, and G. Huang, Opt. Express **21**, 32053 (2013).
- [39] Y.N. Joglekar and B. Bagchi, J. Phys. A **45**, 402001 (2012).